Annual Review of Neuroscience

Fluorescence Imaging of Neural Activity, Neurochemical Dynamics, and Drug-Specific Receptor Conformation with Genetically Encoded Sensors

Chunyang Dong,[1,2,*] Yu Zheng,[3,*] Kiran Long-Iyer,[2,4] Emily C. Wright,[2] Yulong Li,[3] and Lin Tian[2]

[1]Graduate Program in Biochemistry, Molecular, Cellular, and Developmental Biology, University of California, Davis, California, USA

[2]Department of Biochemistry and Molecular Medicine, School of Medicine, University of California, Davis, California, USA; email: lintian@ucdavis.edu

[3]State Key Laboratory of Membrane Biology, Peking University School of Life Sciences; PKU-IDG/McGovern Institute for Brain Research; and Peking-Tsinghua Center for Life Sciences, Beijing, China; email: yulongli@pku.edu.cn

[4]Neuroscience Graduate Program, University of California, Davis, California, USA

Annu. Rev. Neurosci. 2022. 45:273–94

The *Annual Review of Neuroscience* is online at neuro.annualreviews.org

https://doi.org/10.1146/annurev-neuro-110520-031137

*These authors contributed equally to this article

Keywords

fluorescence imaging, genetically encoded indicators, biosensors, drug discovery, neuromodulation, neurocircuit imaging

Abstract

Recent advances in fluorescence imaging permit large-scale recording of neural activity and dynamics of neurochemical release with unprecedented resolution in behaving animals. Calcium imaging with highly optimized genetically encoded indicators provides a mesoscopic view of neural activity from genetically defined populations at cellular and subcellular resolutions. Rigorously improved voltage sensors and microscopy allow for robust spike imaging of populational neurons in various brain regions. In addition, recent protein engineering efforts in the past few years have led to the development of sensors for neurotransmitters and neuromodulators. Here, we discuss the development and applications of these genetically encoded fluorescent indicators in reporting neural activity in response to various behaviors in different biological systems as well as in drug discovery. We also report a simple model to guide sensor selection and optimization.

Contents

INTRODUCTION

To study neural circuitry, the action of one cell within a network of others, one would precisely measure and perturb specific neuronal populations and molecules, which are engaged in performing the computation or function of interest, in behaving animals. The discovery and heterogeneous expression of green fluorescent protein (GFP) promoted the development of a vast array of genetically encoded sensors that have been created to monitor neurotransmission, synaptic spillover, excitable membrane potential, calcium dynamics, vesicle trafficking, receptor mobilization, and other biochemical events. For example, the development of genetically encoded calcium indicators (GECIs) such as GCaMP and its color variant jRGECO, combined with advanced imaging modalities, has revolutionized systems neuroscience (Chen et al. 2013, Dana et al. 2016, Tian et al. 2009) by permitting mesoscopic recording of intracellular calcium as a proxy for electrical activity (Grienberger & Konnerth 2012). Genetically encoded or hybrid voltage indicators (GEVIs) have also been engineered and significantly improved to directly report spiking patterns and subthreshold voltage activity. In addition, genetically encoded sensors for specific neurochemicals report release dynamics with high spatiotemporal resolutions and molecular specificity. Collectively, application of these sensors provides new opportunities for in vivo dissection of neural circuits underlying behavior across various species. In this review, we outline a workflow for sensor development, provide a simple model to guide sensor selection and optimization, and discuss a broad range of applications in neuroscience and pharmacology.

IMAGING NEURONAL ACTIVITY IN GENETICALLY DEFINED POPULATIONS

The GECIs can be categorized into two types based on Förster resonance energy transfer (FRET) between two fluorescent proteins (FPs) or intensity changes of single FPs (**Figure 1*a***). Miyawaki et al. (1997) engineered the very first FRET-based calcium sensor, Cameleon, composed of a calcium-sensitive calmodulin (CaM) and a CaM-binding peptide, M13, sandwiched by two GFP variants (BFP-GFP or CFP-YFP). Calcium binding induces CaM-M13 interaction to increase the FRET efficiency, reflected by changes in the dual emission of donor and acceptor. Further improvements on such FRET-based sensors include chromophore orientation tuning with Venus

variants to improve the response dynamic range (Nagai et al. 2004) and CaM-M13 replacement with troponin C (TnC) or structure-guided redesign of the CaM-M13 interface to minimize cellular perturbation (Mank et al. 2008, Palmer et al. 2006). The ratiometric measurement of such FRET sensors confers correction of motion and blood flow artifacts and allows quantification of intracellular calcium concentration. However, FRET sensors often show less sensitivity compared with single FP–based calcium sensors.

The emergence of single FP–based calcium sensors originates from the creation of circularly permuted fluorescent protein (cpFP) (Baird et al. 1999). The environment-sensitive cpFP can be modulated by the calcium binding–induced conformational changes of CaM-M13/RS20. Early versions of the cpFP-based calcium sensors include Pericam and GCaMP, both using the CaM and M13, with a circularly permuted yellow fluorescent protein or circularly permuted green fluorescent protein (cpGFP) inserted (Nagai et al. 2001, Nakai et al. 2001). Iterative protein evolution has greatly improved the sensors' sensitivity and pushed them into practical use in vivo. In particular, GCaMP6, a big breakthrough in this field, has been widely used in the neuroscience community

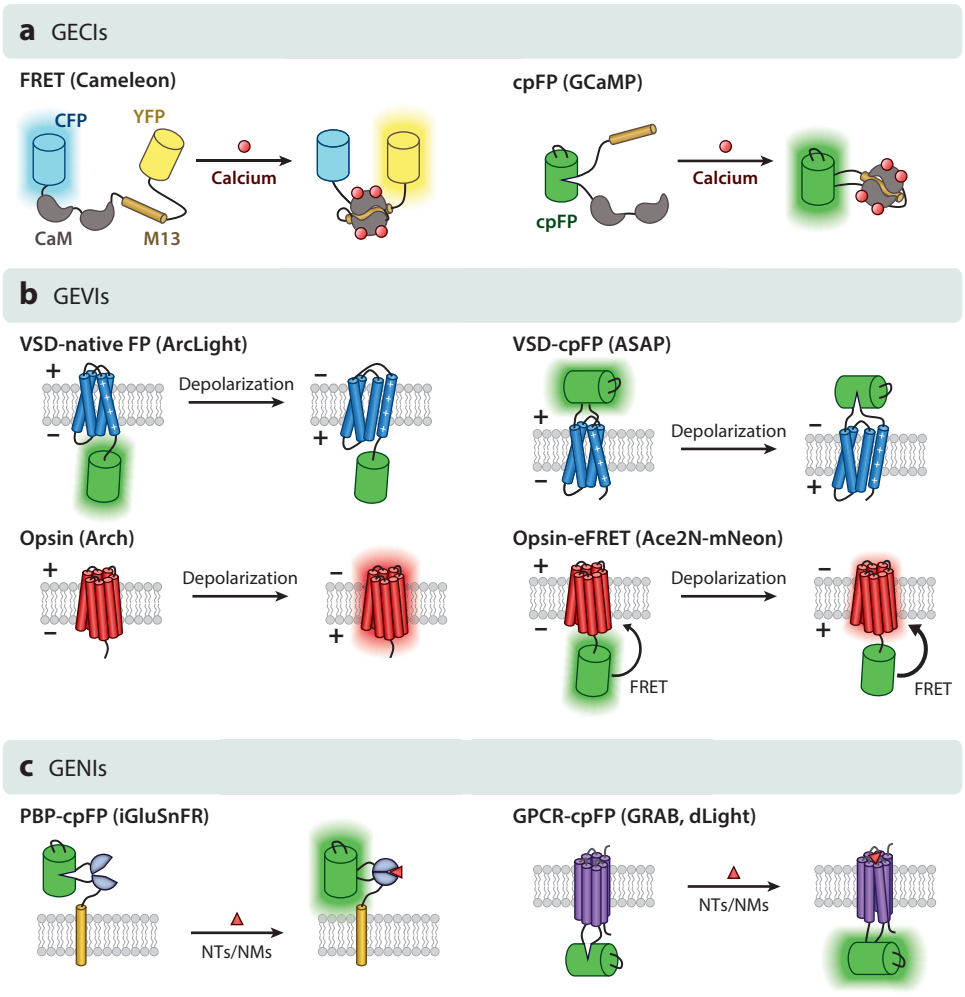

(*Caption appears on following page*)

Figure 1 (*Figure appears on preceding page*)

Schematic representation of genetically encoded indicators for calcium (GECIs), voltage (GEVIs), and neurochemicals (GENIs). (*a*) GECIs are based on Förster resonance energy transfer (FRET) and circularly permuted fluorescent protein (cpFP). The FRET-based calcium sensor is developed by inserting the calmodulin (CaM)-M13 in between donor and acceptor fluorophores such as CFP-YFP or BFP-GFP (e.g., Cameleon). The cpFP-based sensor is intensiometric, in which a cpFP is inserted in between CaM and M13/RS20 (e.g., GCaMP). (*b*) GEVIs utilize the voltage-sensitive domain (VSD) or opsin as scaffold. VSD-based sensors are developed by attaching a native fluorescent protein (FP) to the C terminus of VSD (e.g., ArcLight) or inserting a cpFP into the extracellular S3–S4 loop of the VSD (e.g., ASAP series). The light-driven proton pumps (opsin) are functionally reversed to action as a voltage-sensitive optical element (e.g., Arch). A bright FP is attached to the opsin to address the dimness of opsin-based GEVIs via electrochromic FRET (eFRET), as shown in Ace2N-mNeon. The FP is replaced with HaloTag–Janelia Fluor dyes to develop a hybrid voltage sensor, namely Voltron. (*c*) Two classes of ligand-binding scaffolds, periplasmic binding proteins (PBPs) and G protein–coupled receptors (GPCRs), are used to develop GENIs. In both cases, a cpFP is inserted into the hinge region of PBPs (e.g., iGluSnFR) or intracellular loop 3 of GPCRs (e.g., GRAB, dLight). Abbreviations: NM, neuromodulator; NT, neurotransmitter. Sources for sensors named in the figure are as follows: Cameleon (Miyawaki et al. 1997), GCaMP (Nagai et al. 2001), ArcLight (Jin et al. 2012), ASAP series (St-Pierre et al. 2014, Villette et al. 2019, Yang et al. 2016), Arch (Kralj et al. 2011), Ace2N-mNeon (Gong et al. 2015), Voltron (Abdelfattah et al. 2019), iGluSnFR (Marvin et al. 2013), GRAB (Sun et al. 2018), and dLight (Patriarchi et al. 2018).

for neural activity imaging due to its superior signal-to-noise ratio (SNR) when probing calcium in individual neurons as well as in ensembles in vivo (Chen et al. 2013). Further optimization of GCaMP6 has led to jGCaMP7 and jGCaMP8 series. The jGCaMP7 shows further improved sensitivity and bright basal fluorescence, allowing high-quality calcium imaging in spines and somas (Dana et al. 2019). The latest jGCaMP8 was engineered by swapping the M13 peptide with an endothelial nitric oxide synthase peptide (Zhang et al. 2020). The rational design confers faster kinetics to the sensor, which benefits the tracking of action potentials. A similar strategy was also applied in developing the XCaMP series, in which the M13 was replaced by a ckkap peptide from the neuronal protein CaMKK, which is shown to respond to calcium linearly (Inoue et al. 2019).

Subcellularly targeted GECIs have also been developed to improve the SNR of calcium imaging. Axon-GCaMP6 is a specialized GECI that enriches axonal structures by fusing growth-associated protein-43 (GAP43) (El-Husseini et al. 2001) at the N-terminus of GCaMP6m. Axon-GCaMP enabled the in vivo recording of orientation and direction tuning of axons projecting from L4 V1 neurons across cortical layers without somatodendritic calcium signal contamination (Broussard et al. 2018). The expression of GECIs can also be restricted to neuronal soma to reduce overlapping fluorescence from surrounding neuropil to substantially improve the SNR and specificity of imaging (Chen et al. 2020).

In addition, red-shifted, far-red, and near-infrared (NIR) GECIs have been developed to enable multiplex imaging and to potentially enhance imaging depth, allowing researchers to explore previously unreachable brain regions. R-GECO1 and RCaMP1 were the first red-shifted GECIs designed by replacing cpGFP in GCaMPs with cpmApple and cpmRuby, respectively (Akerboom et al. 2013, Zhao et al. 2011). Further optimization has generated the broadly used jRGECO1a, jRCaMP1a, and jRCaMP1b (Dana et al. 2016). The jRGECO1a is more sensitive but suffers from blue light–induced photoactivation and lysosomal accumulation. A new variant called KGECO1, based on cpFusionRed, was engineered to tackle this issue, while retaining high response (Shen et al. 2018). The color spectrum was further shifted to far red in FR-GECO using the monomeric far-red FP mKelly to enable sensitive detection of single action potentials in neurons (Dalangin et al. 2020).

Recent breakthroughs in protein engineering efforts have also led to the development of non-GFP-based NIR GECIs (Shcherbakova et al. 2015). Taking advantage of biliverdin-binding NIR

FPs, the first NIR GECI, NIR-GECO1, was designed by inserting the CaM-RS20 module into the split NIR mIFP (Qian et al. 2019, 2020). A brighter, FRET-based NIR GECI, named iGECI, utilized two bright NIR FPs, miRFP670 and miRFP720, flanking the CaM-RS20 for FRET (Shemetov et al. 2021). Further optimization in the brightness and photostability of these sensors would significantly improve the SNR for in vivo imaging.

GEVIs, based on the voltage-sensing domain of voltage-sensitive phosphatases or light-driven proton pumps (opsin), have been developed to directly resolve firing patterns and coding properties of targeted neurons such as rapid sequential firing, hyperpolarizing, and subthreshold depolarizing (Knopfel & Song 2019). These GEVIs are engineered to measure membrane potential (V_m) changes (**Figure 1*b***). Though voltage imaging remains challenging compared to calcium imaging, recent rigorous sensor engineering efforts have enabled spiking imaging in genetically defined neuronal populations in behaving animals.

The development and applications of GEVIs have been reviewed extensively and in great depth elsewhere (Pal & Tian 2020, Panzera & Hoppa 2019, Wang et al. 2019). The current GEVIs are still far from optimal. Inadequate sensitivity, along with the requirement of kilohertz acquisition and very limited imaging duration, has limited their utilization to a few laboratories. We expect a practically useful GEVI, in conjunction with GECIs, to provide more precise dissection of information processing in the brain. Nevertheless, GECIs and GEVIs have paved the way for genetically encoded indicators, providing the foundation for the engineering and application of other sensors, including the neurochemical sensors reviewed below.

IMAGING BEYOND SPIKES WITH NEUROTRANSMITTER AND NEUROMODULATOR SENSORS

Neurotransmitters (NTs) and neuromodulators (NMs) are essential signaling molecules for information processing in the brain. There are more than 100 known NT and NM molecules (Kovacs 2004), classified as amino acids, monoamines, neuropeptides, purines, and lipids based on their structures. Fast-acting NTs, namely glutamate and gamma-aminobutyric acid (GABA), act through ligand-gated ion channels and G protein–coupled receptors (GPCRs) to modulate firing rate and excitability of postsynaptic cells. In contrast to fast-acting NTs, NMs almost exclusively bind to GPCRs to initiate molecular signaling cascades that modulate synaptic strength, neuronal excitability, and circuit dynamics on timescales of subseconds to hours (Guillaumin & Burdakov 2021, Nadim & Bucher 2014). Altered NT and NM release is central to the pathogenesis of neurological and psychiatric disorders. Although the anatomical characterizations of NT and NM projections and their functional significance are understood at a moderate level, many outstanding questions remain regarding the structural and molecular basis and key computations underlying their release. There is a pressing need to increase experimental capacity to precisely measure the dynamics of these molecules with subsecond and single-cell resolution, high molecular specificity, and cell type specificity, ideally, across the full course of a behavioral paradigm.

Inspired by the design of GECIs, we and others have developed a tool kit of genetically encoded single FP–based indicators to probe various NT and NM systems (**Figure 1*c***). To date, two main categories of single FP sensors have been developed, classified by their ligand-binding scaffolds: bacterial periplasmic binding proteins (PBPs) and GPCRs.

PBP scaffolds are attractive for sensor engineering due to the conserved and large conformational change of PBP upon ligand binding. These proteins usually consist of two domains linked by a hinge region; this structure is conserved across other PBPs (Quiocho & Ledvina 1996). The ligand binding site is located in between the two domains, and the protein typically adopts two distinct conformations: a ligand-free (Apo) and a ligand-bound (Sat) state. These two conformations can interconvert via the hinge region upon ligand binding and releasing. By connecting these

PBPs with a cpFP, we can achieve more versatile and intensiometric measurements of the ligand transients in real time. Using this design platform, highly sensitive sensors have been developed for glutamate [iGluSnFR (Helassa et al. 2018; Marvin et al. 2013, 2018)]; acetylcholine [iAChSnFR (Borden et al. 2020)]; GABA [iGABASnFR (Marvin et al. 2019)]; nicotine [iNicSnFR (Shivange et al. 2019)]; ATP [iATPSnFR (Lobas et al. 2019)]; glucose (Hu et al. 2018, Keller et al. 2021, Mita et al. 2019); and, more recently, serotonin [iSeroSnFR (Unger et al. 2020)].

The development of iGluSnFR pioneered the field of NT sensor development and paved the way for developing other NT/NM sensors. For example, the acetylcholine sensor, iAChSnFR, consists of a hyperthermophilic homolog of *Bacillus subtilis* OpuBC from *Thermoanaerobacter* sp. *X513* and a circularly permuted superfolder green fluorescent protein (cpSFGFP) (Borden et al. 2020). A critical challenge for developing iAChSnFR is the specificity tuning. The *X513*-OpuBC binds to both choline and acetylcholine, and the affinity for choline ($k_d = 8$ uM) is tighter than that for acetylcholine ($k_d = 95$ uM). With the guidance of crystal structure modeling and modifications on the binding pockets, hinge region, protein interface between *X513* and cpSFGFP, and junctions between the binding protein and cpSFGFP, the specificity and affinity of iAChSnFR have shifted from choline toward acetylcholine, despite the molecular similarity between the two. Expressing iAChSnFR in HEK293T cells yields an apparent k_d of 2.9 ± 1.6 uM and a maximum dynamic range of 10 ± 1.4 folds. Furthermore, iAChSnFR has been utilized for in vivo recordings in mice, fish, flies, and worms (Borden et al. 2020).

The recent development of the PBP-based serotonin sensor iSeroSnFR furthered the process of altering specificity and selectivity of the binding protein. By applying a machine learning strategy and computational modeling, the binding pocket of iAChSnFR was radically redesigned to bind serotonin while ablating acetylcholine and choline binding. The finalized iSeroSnFR conveys 19 mutations with an approximately 5,000-fold increase in serotonin binding specificity compared to iAChSnFR. The large dynamic range of this sensor permits in vivo detection of distinct serotonin transients across various brain regions and behaviors, including fear conditioning and sleep-wake cycles (Unger et al. 2020).

Endeavors to create genetically encoded sensors based on GPCRs as a binding module have started to further expand the toolbox (Andreoni et al. 2019, Sabatini & Tian 2020, Wang et al. 2018). Not only are GPCRs the largest and most diverse group of membrane receptors in eukaryotes, but they are also native targets of NTs and NMs in the brain. The readily available binding module for endogenous NTs and NMs of interest, as well as their highly conserved structures, led to the development of a universal design approach for NM sensors. The existing GPCR structures combined with computational simulation approaches suggest that the largest conformational change upon ligand binding is in the intracellular loop 3 (ICL3), the domain crucial for recruiting G proteins, which lies in between transmembrane (TM) domains TM5 and TM6 (Tikhonova & Costanzi 2009) (for solved GPCR structures, see Zhang et al. 2015). Two major single-FP intensiometric sensors, the Light and GRAB families, have been developed utilizing this conformational change. The general design strategies for GPCR-based sensors are similar to the PBP-based sensors, except they use the binding moiety from GPCRs. For the dLight1 series, based on three dopamine (DA) receptors (DRD1, 2, and 4), ICL3 of various DA receptors was completely removed and the cpGFP was inserted directly onto the TMs with short linkers (Patriarchi et al. 2018), while the GPCR activation–based dopamine sensor ($GRAB_{DA}$) series, based on the DRD2 receptor used different linkers and ICL3 insertion sites (Sun et al. 2018). By systematic site saturation mutagenesis (SSM) on the linker region, GFP, and receptors, dLight1 achieved an affinity range from 4 nM to 2.3 μM, with a dynamic range from 170% to 930%. Similarly, $GRAB_{DA}$ has an affinity of 7–130 nM and a dynamic range from 90% to 340%. The high affinity and high specificity of the DA sensors demonstrated excellent fluorescent sensitivity and brightness

in response to ligand binding, making them ideally suited for in vivo imaging. This strategy has been successfully expanded to generate more GPCR-based biosensors for detecting other NMs, including acetylcholine ($GRAB_{ACh}$), norepinephrine (nLight, $GRAB_{NE}$), serotonin (psychLight, $GRAB_{5\text{-}HT}$), adenosine ($GRAB_{Ado}$), ATP ($GRAB_{ATP}$), and endocannabinoids ($GRAB_{eCB}$) (Dong et al. 2020; Dong et al. 2021; Feng et al. 2019; Jing et al. 2018, 2020; Peng et al. 2020; Wan et al. 2021; Wu et al. 2021).

WORKFLOW FOR DEVELOPMENT AND OPTIMIZATION OF NEUROTRANSMITTER AND NEUROMODULATOR SENSORS

Despite the considerable progress in NT/NM sensors that has been made in recent years, the existing NTs with applicable sensors are still far from adequate. Here, we summarize the workflow of how to develop and optimize NT/NM sensors, with $GRAB_{DA}$ as an example, aiming to facilitate the expansion of sensor families (Sun et al. 2018, 2020) (**Figure 2**).

The first step is choosing a good sensing domain that will determine the overall performance of the sensor (**Figure 2*a***). GPCRs are more desirable due to the lack of the corresponding PBPs for most NT/NMs like DA. Moreover, diverse subtypes of GPCRs offer more choices. A potential candidate should be evaluated according to a set of criteria, including membrane trafficking, affinity and selectivity, and the initial dynamic range. During the development of $GRAB_{DA}$ sensors, DRD1 and DRD2 showed excellent membrane trafficking when cpGFP was inserted in the preliminary screening of five human DA receptor subtypes. DRD2 was chosen for $GRAB_{DA}$ sensors because of its higher affinity than DRD1, while DRD1 was chosen as the scaffold for dLight sensors due to its higher selectivity of DA over norepinephrine (as shown in the dLight1.3b sensor). GPCRs from different species or GPCR redesign by the computational approach also provides additional options.

In order to create an effective sensor with a high SNR, it is imperative to maximize the dynamic range, defined as fluorescent response elicited by ligand binding. One practical approach to amplify the transduction of conformational change to the fluorescent domain is systematic truncation of the ICL3. This strategy helps determine the appropriate position of cpGFP insertion into the GPCRs. After cpGFP insertion, SSM on the linker residues between the FP domain and the receptor scaffold is utilized to generate a library of sensor variants (**Figure 2*b***). This method was used to engineer the $GRAB_{DA1m}$ sensor, yielding a maximal dynamic range of about 90%. Further optimization of $GRAB_{DA}$ can firstly focus on the cpGFP, especially on the interface with a GPCR. Other potential sites on the cpGFP can be obtained from the differential sites in alignment with brighter GFP variants, such as sfGFP and mClover3, or cpGFP variants from other sensors, including GECIs and GEVIs. A two- to threefold improvement in response was observed in this step for the next-generation $GRAB_{DA}$ sensors. These steps are not always sequential. Sometimes, individual optimization of the linker region and cpGFP followed by a combination of beneficial mutations may help to maximize the sensitivity, as presented in the development of $GRAB_{ACh3.0}$ (Jing et al. 2020).

Dynamic range and brightness are the priorities for the previous steps. Additional parameters should be considered, including affinity, kinetics, and color expansion, as they also determine the in vivo performance (**Figure 2*c***). The affinity can be tuned by rational design on the ligand-binding pocket to match the concentration of NT release in physiological conditions in vivo, in which the resolved structures are of great help. In addition, previous downstream functional analysis also provides potential sites for affinity tuning, especially as some of them are outside of the ligand-binding pocket. For example, in the $GRAB_{DA}$ sensor, the T205M mutation on DRD2 that was previously identified by evolution-based computational approaches and validated by downstream

signaling detection assay was introduced to generate high-affinity versions (Sung et al. 2016). Fast on and off kinetics are always expected for sensors, but there usually exists a compromise between kinetics and affinity. For example, the high-affinity $GRAB_{DA1h}$ and $GRAB_{DA2h}$ show a slower off rate than do low-affinity $GRAB_{DA1m}$ and $GRAB_{DA2m}$, respectively. The color of sensors can be

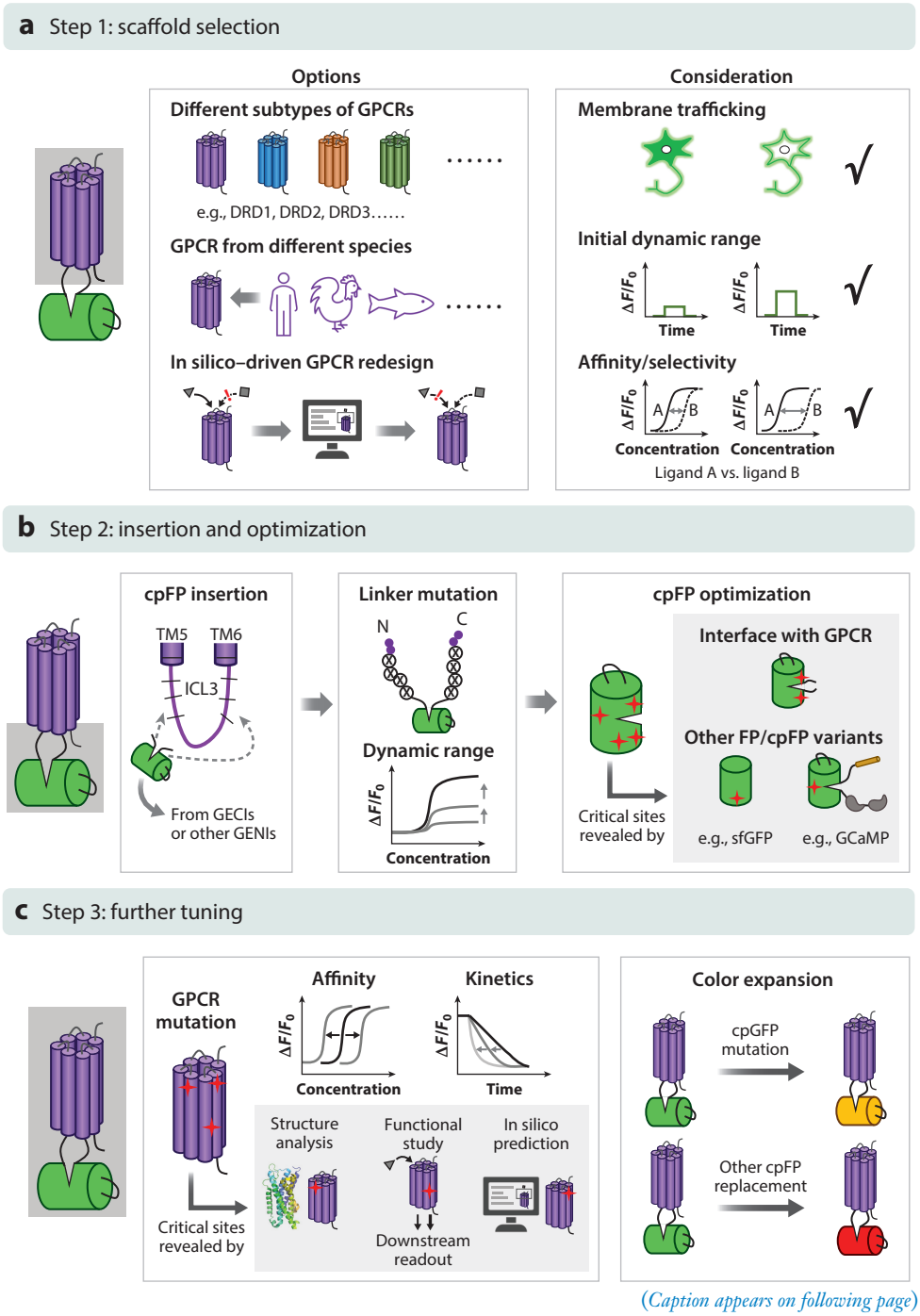

(*Caption appears on following page*)

Figure 2 (*Figure appears on preceding page*)

A workflow for the development and optimization of GPCR-based neurochemical sensors. (*a*) Options and considerations for selecting an appropriate GPCR scaffold. GPCRs can be from different subtypes, from different species, and redesigned in silico. A good scaffold should show good membrane trafficking, high initial dynamic range after cpFP insertion, appropriate affinity, and high selectivity for the neurochemical of interest. (*b*) After choosing a good scaffold, cpFP insertion site optimization, linker optimization, and cpFP optimization can be performed sequentially. The critical sites in cpFP optimization are mainly on the interface with the GPCR or learned from other FP or cpFP variants, as highlighted in gray. (*c*) Further tuning can be performed by mutating GPCRs to tune the affinity and kinetics. The potential sites in GPCRs can be obtained from the reported GPCR structures, previous functional studies by downstream signaling detection, and in silico prediction, as highlighted in gray. The color can be expanded by introducing several mutations to the cpGFP or by replacing it with other cpFPs (e.g., cpmApple). Abbreviations: cpFP, circularly permuted fluorescent protein; cpGFP, circularly permuted green fluorescent protein; FP, fluorescent protein; GECI, genetically-encoded calcium indicator; GENI, genetically encoded neurochemical indicator; GPCR, G protein–coupled receptor; ICL3, intracellular loop 3; sfGFP, superfolder green fluorescent protein; TM, transmembrane.

slightly yellow-shifted by introducing a mutation on cpGFP or further red-shifted by replacing them with other cpFPs such as cpmApple, which is used to develop red $GRAB_{DA}$ sensors.

THEORETIC CONSIDERATIONS TO CHOOSE AND OPTIMIZE SENSORS

No tool is without its limitations. GPCR-based sensors have similar ligand affinity to endogenous receptors, which may reduce effective dynamic range and interfere with endogenous signaling pathways. PBP-based sensors, on the other hand, have large dynamic range but may have compromised sensitivity at lower concentrations of release. The appropriate combination of intrinsic parameters of a sensor, including brightness, expression, dynamic range, apparent affinity, and kinetics, must be matched to the extrinsic properties of the system, which include the size, shape, and frequency and concentration of release. To guide the selection of the sensor that is most appropriate to applications and future improvement, especially for NM sensors, we provide a simple model based on kinetics and dynamic ranges of $GRAB_{5\text{-}HT1.0}$ and iSeroSnFR that illustrates the relationship between these parameters (**Figure 3**).

We define the dissociation and association rates of receptor or sensor and yield k_d as a rate constant at half of the maximum dynamic range:

$$k_{d_R} = \frac{[Ligand] \bullet [Receptor]}{[Ligand \cdot Receptor]} = \frac{k_{off_R}}{k_{on_R}}, \quad 1.$$

$$k_{d_S} = \frac{[Ligand] \bullet [Sensor]}{[Ligand \cdot Sensor]} = \frac{k_{off_S}}{k_{on_S}}. \quad 2.$$

When k_d of the sensor is similar to the endogenous receptor, we need to factor in the competition of ligand binding. We thus define f as the ratio of the fractional occupancy of sensor and native receptor with respect to ligand concentration, in which fractional occupancy (Θ) is defined as the fraction of receptors in a bound state (Motulsky & Neubig 2010):

$$f = \frac{\Theta_{[Ligand \cdot Sensor]}}{\Theta_{[Ligand \cdot Receptor]}} = \frac{[Sensor] \bullet \left(k_{d_R} + [Ligand]\right)}{[Receptor] \bullet \left(k_{d_S} + [Ligand]\right)}. \quad 3.$$

We next define $\frac{\Delta F}{F}$ as the sensor's fluorescence change relative to its baseline fluorescence based on ligand binding, where F is fluorescence intensity. According to the specific binding equation,

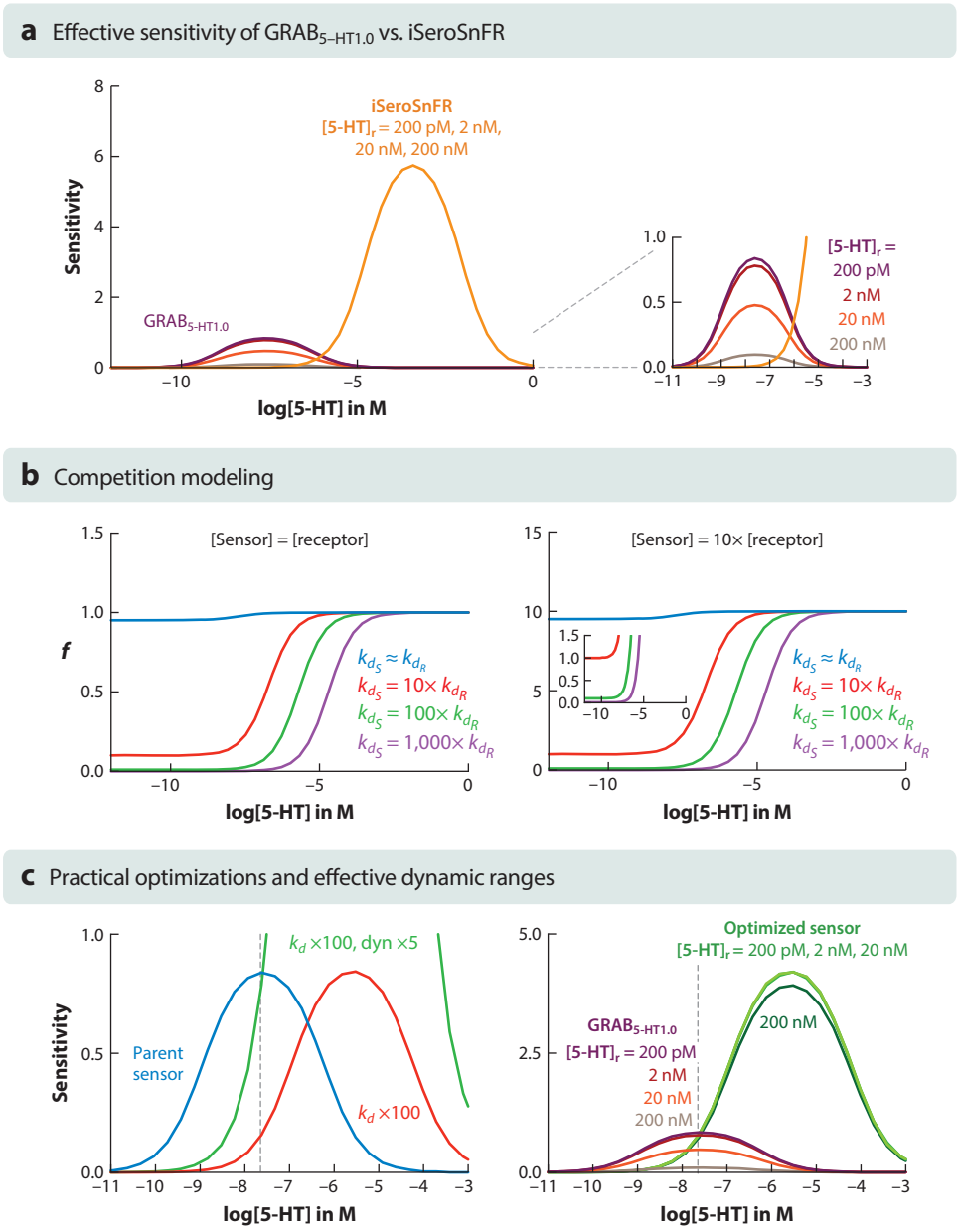

Figure 3

Computational modeling to guide sensor optimizations. (*a*) Modeling of effective sensitivity of $GRAB_{5\text{-}HT1.0}$ (*magenta*) and iSeroSnFR (*yellow*) at resting serotonin concentration ($[5\text{-}HT]_r$) of 200 pM, 2 nM, 20 nM, and 200 nM. (*b*) A 100-fold (*green*) or greater increase in sensor k_d relative to that of the native receptor minimizes ligand buffering effect when sensor and receptor expression are equal (*left*) and when sensor expression is 10 times higher than receptor expression (*right*). (*c*, *left*) A practical optimization for $GRAB_{5\text{-}HT1.0}$ to maintain or enhance sensitivity while minimizing competition is to increase both the k_d and the maximum dynamic range of the parent sensor (*blue*). According to the model, this can be achieved with a 100-fold increase in k_d and a 5-fold increase in maximum dynamic range (*green*). (*Right*) The optimized sensor is more tolerant to changes in $[5\text{-}HT]_r$ compared to the parent $GRAB_{5\text{-}HT1.0}$, while maintaining similar sensitivity at the ligand concentration where the parent $GRAB_{5\text{-}HT1.0}$ sensor has the peak sensitivity.

we can obtain a function of $\frac{\Delta F}{F}$ with respect to ligand concentration:

$$\frac{\Delta F}{F_{([Ligand])}} = \frac{F_{([Ligand])} - F_{([L]_0)}}{F_{([L]_0)}} = \frac{\left(\frac{\Delta F}{F}\right)_{max} \bullet [Ligand]}{k_{d_S} + [Ligand]}. \quad 4.$$

We assume both PBP-based sensors and GPCR-based sensors have a Hill coefficient of one. $F_{([Ligand])}$is a function of fluorescence intensity with respect to ligand concentration. $F_{([L]_0)}$ is a constant calculated from the function $F_{([Ligand])}$ when ligand concentration is zero. $(\frac{\Delta F}{F})_{max}$is the maximum dynamic range of the sensor at its saturation ligand concentration.

This leads to the definition of the sensitivity of the sensor as the first derivative of function $\frac{\Delta F}{F([Ligand])}$:

$$\frac{\partial \frac{\Delta F}{F}([Ligand])}{\partial [Ligand]} = \frac{\left(\frac{\Delta F}{F}\right)_{max} \bullet k_{d_S}}{\left(k_{d_S} + [Ligand]\right)^2}. \quad 5.$$

When the resting ligand concentration is above zero, the effective sensitivity is affected. We finally define the effective sensitivity as

$$\frac{\partial \frac{\Delta F}{F}([Ligand])}{\partial [Ligand]}' = \frac{\left(\frac{\Delta F}{F}\right)_{([Ligand])}' \bullet k_{d_S}}{\left(k_{d_S} + [Ligand]\right)^2}, \quad 6.$$

where

$$\left(\frac{\Delta F}{F}\right)_{([Ligand])}' = \frac{F_{([Ligand])} - F_{([L]_r)}}{F_{([L]_r)}} = \frac{\left\{\left(\frac{\Delta F}{F}\right)_{max} - \frac{\left(\frac{\Delta F}{F}\right)_{max} \bullet [L]_r}{k_{d_S} + [L]_r}\right\} \bullet [Ligand]}{k_{d_S} + [Ligand]}$$

and $[L]_r$ is resting NM release concentration.

$GRAB_{5\text{-}HT1.0}$ showed much higher sensitivity at a range of 1 nM to 1 μM compared to iSeroSnFR, while the sensitivity started to decrease when the release concentration was beyond 10 nM (**Figure 3*a***). However, the effective sensitivity of $GRAB_{5\text{-}HT1.0}$ significantly decreases with the increase of extracellular ligand concentration at equilibrium, whereas the effective sensitivity of iSeroSnFR remains unchanged (**Figure 3*a***). Therefore, it is concerning that $GRAB_{5\text{-}HT1.0}$ may have compromised sensitivity when the extracellular serotonin concentration is higher at resting state. In contrast, iSeroSnFR would theoretically be less affected by resting concentration. Both serotonin sensors have shown capabilities of recording in vivo (Unger et al. 2020, Wan et al. 2021); iSeroSnFR may not fully utilize its dynamic range at nanomolar release range, whereas $GRAB_{5\text{-}HT1.0}$ could potentially encounter saturation. In other words, the intrinsic properties of both sensors can be further optimized.

As the dissociation rate of $GRAB_{5\text{-}HT1.0}$ is similar to the endogenous 5-HT2 receptor (k_d of 5-HT2R = 20 nM) (Kelly & Sharif 2006), the potential competition with the endogenous receptor can be predominant, especially for long-term expression. Based on the model, if a sensor's dissociation rate can be increased about 100-fold higher than the endogenous receptor, the competition at the physiological range of release is minimal, which will significantly reduce the potential buffering effect (see the left side of **Figure 3*b***). However, by simply increasing the dissociation rate, the sensitivity of the sensor will be reduced (see the left side of **Figure 3*c***). To compensate for the loss of sensitivity, we also need to increase the dynamic range. Therefore, to maximize the effective sensitivity with minimal buffering, a practical optimization goal for $GRAB_{5\text{-}HT1.0}$ is to increase the k_d by 100-fold while increasing the dynamic range by fivefold as predicted by the model

(see the right side of **Figure 3*c***). On the other hand, to optimize iSeroSnFR, the model is predicted to decrease its k_d by 100-fold while maintaining the dynamic range. Theoretically, if the dynamic range of iSeroSnFR can be further increased by fivefold, the sensitivity would be able to detect the release between 100 nM and 1 mM without compromised effective sensitivity or buffering effect. However, this ideal sensor may be practically difficult to engineer.

The other important factor affecting the SNR of imaging is the expression level of the sensor. We assume that the arbitrary sensor concentration is 10 times higher than that of native receptors to achieve sufficient SNR. Thus, the fraction will upshift and be more favorable to sensors than to endogenous receptors. However, a 100-fold-higher k_d is still able to minimize the competition even when the sensor expression level is 10 times higher than that of the endogenous receptors (see the right side of **Figure 3*b***). By increasing the maximum dynamic range and basal fluorescence, we can boost effective sensitivity at the lower release concentration. This modeling did not account for diffusion rate, distance of diffusion, ligand removal from transporter or enzyme, and assuming equilibrium is reached when binding. Together, our model suggests that an ideal sensor for a ligand of interest should have high dynamic range combined with a relatively higher dissociation rate compared to endogenous ligand-binding receptors. To practically achieve these end points, we have proposed a few strategies outlined in the workflow above. While optimizing both sensitivity and dynamic range can be guided by rational design, high-throughput screening of variants properties is needed, which can be a potential roadblock during the course of sensor optimization, especially for membrane-bound sensors. An optimal tool development pipeline requires both theoretical and experimental methods to engineer a sensor with great sensitivity and fast kinetics, while minimizing buffering effects.

IMAGING NEUROMODULATOR RELEASE IN BEHAVING ANIMALS

The fast-growing tool kit of genetically encoded sensors has allowed researchers to study complex neural systems and circuitry across a range of animal models with flexible experimental design. These tools are optimally tuned to answer biological questions about the functionality, pharmacology, and interactions of different molecules involved in chemical neurotransmission. One of the primary advantages is the subsecond temporal resolution. This allows real-time alignment of neural activity across the full course of behaviors. Additionally, the use of spectrally separated sensors permits great flexibility in experimental design, as the sensors can be multiplexed to record and compare transients from different neurochemicals simultaneously (Patriarchi et al. 2020, Sun et al. 2020). For example, researchers can use calcium indicators in conjunction with NM and NT sensors to interrogate the interplay of cellular activity and different neurochemical release phenomena.

Genetically encoded sensors offer the unique advantage of cell type–specific viral strategies for targeting distinct neuronal populations. Researchers can use a host of approaches to narrow the scope of sensor expression. Promoters such as CaMKII and hSyn are often utilized for broad distinction of neurons (Kügler et al. 2003, Nieuwenhuis et al. 2021, Wang et al. 2013). Viral constructs can also be expressed under promoters designed to localize expression to subclasses of neurons, e.g., the GAD67 promoter selectively expresses in GABAergic neurons (Rasmussen et al. 2007). For additional specificity, researchers can employ transgenic animal models to limit sensor expression. Gene recombination systems, such as Cre/lox, are widely used to constrain sensor expression to specific cell types (Bouabe & Okkenhaug 2013, Kim et al. 2018). These approaches are generally combined with local or systematic viral injections to selectively label and image from region- or projection-specific cell types at scale.

The array of existing sensors combined with various imaging modalities provides an expanded technical arsenal for the interrogation of neural circuits, systems, and behaviors. Fiber photometry

combined with genetically encoded sensors enables subsecond recording of calcium and neurochemical dynamics in freely moving, behaving rodents and elucidates neurobiological phenomena underlying innate and learned behaviors, albeit with a lack of single-cell resolution (Sabatini & Tian 2020). Additionally, photometric recording is suitable for targeting deep subcortical nuclei and densely fasciculated projections, which are difficult to access with either one- or multiphoton microscopy. For example, adenosine ($GRAB_{Ado}$) and serotonin ($GRAB_{5\text{-}HT}$ and iSeroSnFR) sensors have revealed fluctuating dynamics of extracellular adenosine and serotonin, respectively, over the entire course of the sleep-wake cycle in mouse cortical and subcortical regions (Unger et al. 2020) (**Figure 4*a***). With fiber photometry, dLight has been used to great effect to understand downstream effects of dopaminergic neuromodulation. Recent work in the field of neural reinforcement learning illustrated a dissociation between dopaminergic ventral tegmental area (VTA) spiking and DA release in the nucleus accumbens (NAc) using dLight. The authors showed that DA release in the NAc core covaried with reward history and expectations independent of dopaminergic VTA neuron spiking (Mohebi et al. 2019). Other research has revealed that positive and negative DA modulation leads to cell type–specific, asynchronous fluctuations in spiny projection neuron protein kinase A levels (Lee et al. 2021).

One- and multiphoton microscopy combined with NM sensors, on the other hand, provide the cellular or subcellular map of distinct release in response to electrical stimuli or behavior. For example, two-photon imaging of DA with the fast DA sensor dLight1.3b revealed the rise and fall of local synaptic release within 200 ms before the postsynaptic current reached plateau (Condon et al. 2021). Wide-field mesoscopic recordings of $GRAB_{ACh3.0}$ sensors in the primary somatosensory cortex have led to insights on single-cell cholinergic activity within cortical neuron populations in response to systemic pharmacological manipulation (Jing et al. 2020). Additionally, single- and multiphoton microendoscopy techniques have been adapted and optimized for freely moving behavior (Ziv & Ghosh 2015). These adaptations also permit high-resolution imaging in deep brain regions (Zhang et al. 2019). Miniature two-photon microscopy has been used to demonstrate visual cortex cholinergic response during a treadmill task in mice using the $GRAB_{ACh3.0}$ sensor (**Figure 4*b***). It is worth mentioning that the intrinsic properties of current NM sensors need to be further optimized for broad application with all microscopies.

What is particularly exciting about the multitude of ways these sensors can be implemented in vivo is the broad range of novel questions and experimental designs to which they can be applied. A prominent topic in neurobehavioral research that will benefit from the in vivo imaging methods discussed here is social behavior. Social behaviors represent a range of interactions where two or more animals are engaging with each other and relate to a wide array of important and translatable lines of research, including mental health topics (Lim & Young 2006). Researchers have previously encountered roadblocks in measuring neural activity during social behaviors due to the freedom of movement required in many social behavior tests. Recent work has begun to take advantage of recording setups that allow unrestrained movement to investigate circuit-specific activity during behaviors such as neutral interaction (Gunaydin et al. 2014), social defeat (Muir et al. 2018), social isolation (Matthews et al. 2016, Mita et al. 2019), and social reward (Hung et al. 2017). It is even possible to record from multiple animals who are actively interacting and correlate changes in neural activity between animals (**Figure 4*c***). All the examples noted thus far utilize calcium imaging with transgenic Cre lines to ensure cell type specificity. However, the advent of NM and NT sensors allows for specific and meaningful observations of dynamic changes in neurocircuitry to be conducted in model species that do not have transgenic options.

Genetically encoded sensors can be modified and used across an array of different species, both vertebrate and invertebrate. $GRAB_{ACh}$ sensors have been validated in *Drosophila* and mice, and the $GRAB_{DA}$ sensor has been shown to track DA fluctuations in *Drosophila*, zebrafish, and mice

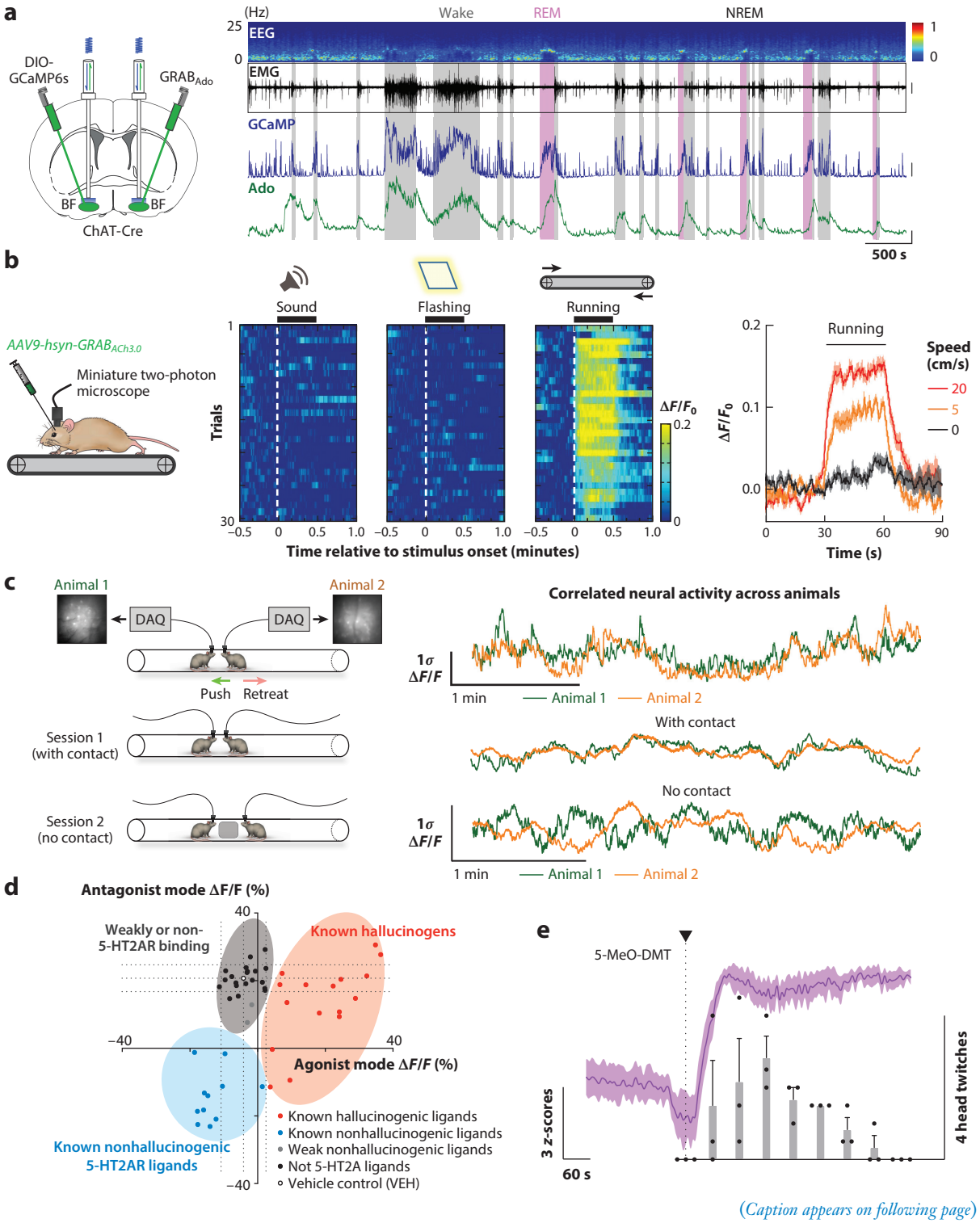

(*Caption appears on following page*)

Figure 4 (*Figure appears on preceding page*)

Behavioral and pharmacological applications of NT/NM sensors. (*a*) Long-term recording of adenosine release in cholinergic neurons using the $GRAB_{Ado}$ sensor. Changes in adenosine-dependent fluorescence can be compared to cholinergic calcium activity and EEG/EMG signal across the full time course of the sleep-wake cycle. Panel *a* adapted from Peng et al. (2020). (*b*) Imaging $GRAB_{Ach3.0}$ sensor using miniature two-photon microscopy in a treadmill task in mice. Single-cell changes in $\frac{\Delta F}{F}$ responses are tractable during different stages of the task and across running speeds. Panel *b* adapted from Jing et al. (2020). (*c*) Simultaneous calcium imaging in dmPFC of two mice during a social interaction test reveals correlations in neural activity during contact versus no contact sessions. Panel *c* adapted with permission from Kingsbury et al. (2019); copyright 2021 Elsevier. (*d*) psychLight-based characterization of compounds based on 5-HT2AR binding and hallucinogenic potential. Panel *d* adapted from Dong et al. (2021). (*e*) psychLight tracks in vivo action of 5-MeO-DMT administration over the course of the head-twitch response. Panel *e* adapted from Dong et al. (2021). Abbreviations: 5-MeO-DMT, 5-methoxy-*N*,*N*-dimethyltryptamine; DAQ, digital acquisition device; dmPFC, dorsomedial prefrontal cortex; EEG, electroencephalography; EMG, electromyography; NM, neuromodulator; NREM, non-rapid eye movement; NT, neurotransmitter; REM, rapid eye movement.

(Jing et al. 2020; Sun et al. 2018, 2020). There are also advantages to using these sensors in wild-type animals, namely that they can serve to better model certain ethology. For example, researchers interested in understanding the neurobiology of paternal behavior may prefer to use mandarin voles as a model, as mandarin voles are one of the few rodent species to show a high level of paternal infant-directed care (Tai & Wang 2001, Tai et al. 2001). Mandarin vole researchers have used the dLight1 sensor to record DA release into NAc during infant-directed paternal behaviors, allowing for specificity of real-time, unrestrained, region-specific NT recording without a need for transgenics (He et al. 2021). Similarly, the $GRAB_{DA}$ was used in zebra finches to monitor DA dynamics in the dopaminergic mesocortical circuit during cultural transmission of vocal behavior (Tanaka et al. 2018). The use of neurochemical sensors in nontraditional models is still in its infancy, but we predict we will see a large increase in popularity. Future studies may see a large increase in the diversity of animal models that allows for the examination of behaviors, conditions, or characteristics not available in inbred lab mice or rats. The California mouse, for example, exhibits high levels of female-female aggression (Trainor et al. 2011) and sex-specific changes in anxiety behavior (Wright et al. 2020), allowing for unique insights into sex differences in anxiety-driven neuromodulation. Forays into sensor application in nonhuman primates have already begun (Sadakane et al. 2015, Seidemann et al. 2016) and represent a future direction of research where sensor neuroimaging could be done in complex cortical regions that do not present in rodents. Neurochemical sensors can be applied in cases like these to probe important questions using the most translatable animal model and ethological experimental design.

Spectrally shifted sensors further push the boundaries of in vivo imaging possibilities. Spatiotemporal overlap in neurochemical release, either from synaptic corelease or from converging inputs, is a common phenomenon but one that has been historically difficult to visualize. By using spectrally distinct sensors, researchers can monitor and correlate activity of multiple neurochemicals without sacrificing spatiotemporal resolution. Red-shifted iGluSnFR (Wu et al. 2018), red- and yellow-shifted dLight (Patriarchi et al. 2020), and red-shifted $GRAB_{DA}$ (Sun et al. 2020) sensors have already been engineered. We recognize the importance of continued efforts to produce an expanded palette of neurochemical sensors and the wide-reaching implications that these developments have on the ability to measure interactions and complexities of in vivo neurochemical systems. Additionally, the universally applied sensor engineering methods can also be used to expand the scope of neurochemical sensors. For example, neurolipid indicators have permitted exploration of clinically relevant neurophysiology of endogenous lipid activity. Namely, the $GRAB_{eCB2.0}$ sensor has revealed in vivo endocannabinoid transients across multiple brain regions in response to foot shock, locomotion, and seizure (Dong et al. 2020, Farrell et al. 2021).

APPLICATION OF NEUROTRANSMITTER SENSORS IN DRUG DISCOVERY

Besides imaging endogenous NM release dynamics, GPCR-based NM sensors such as psychLight have been recently applied to probe specific ligand-induced conformational changes of the 5-HT2A receptor to predict behavioral outcomes. The cell-based high-throughput assays using 5-HT2A now enable early identification of abusive drugs and the development of 5-HT2AR-dependent nonhallucinogenic therapeutics at scale.

Thirty-five percent of all Food and Drug Administration–approved medications bind to GPCRs (Hauser et al. 2017). The size, shape, and amino acid composition of the orthosteric binding site are very well suited to designing small synthetic molecules (Shoichet & Kobilka 2012). The ligand-binding-specific conformation of the receptor dictates its function and diverse behavior via different conformation-dependent downstream pathways. It is known that there are multiple signaling pathways for GPCRs, and it is possible to bias the signaling of a given GPCR through either a specific G protein or through β-arrestin induced by designer compounds (Smith et al. 2018), and the biased agonism on GPCRs has been utilized in pharmacology to reduce the side effects of some designer compounds (Whalen et al. 2011). However, the mechanistic action of designer drugs at both molecular and cellular levels is not known. There is a pressing need to develop technologies that can access drugs with addictive potentials at scale in the early stages of drug discovery.

Recently, an open source of 14 optimized bioluminescence resonance energy transfer (BRET)-based sensors, TRUPATH, has facilitated the understanding of drug actions on GPCRs (Olsen et al. 2020). By attaching a RLuc8 on the optimized location of 14 different Gα units and GFP2 on Gγ units—and BRET can happen only when two fluorophores are in the correct proximation and orientation—TRUPATH can specifically indicate the physical association of combinations of Gα, Gβ, and Gγ. Before binding of ligands, the G proteins are in a heterotrimer state. RLuc8 and GFP2 are in proximity so a BRET signal can be observed. Upon binding, Gα subunit exchanges bound guanosine diphosphate with guanosine triphosphate. The disassociation of the Gα unit from the βγ subunit will result in a loss of BRET signal, which indicates when the specific G proteins that are tagged with FP are being engaged. Thus, one can identify specific transducer complexes that are activated by a specific drug in response to a GPCR of interest. Furthermore, TRUPATH verified that both in wild-type κOR and in chemogenetic κOR Ro1 activated canonical Gαi3 and novel GαGustducin transducers to a similar extent, which was the pathway that was previously reported from in vivo experiments (Mueller et al. 2005).

On the other hand, the use of GPCR-based sensors is a promising strategy to directly monitor the specific receptor conformational changes induced by ligands instead of secondary signaling molecules. The 5-HT2A receptor is the major target of psychedelics, which have shown promising antidepressant, albeit severe hallucinogenic, effects (Chi & Gold 2020). Recent research has shown that the hallucination effect is not necessary for treating depression (Cameron et al. 2021). Thus, it is imperative to screen novel compounds for 5-HT2ARs that do not trigger hallucination but still retain therapeutic effects. To do so, psychLight was engineered by coupling the fluorescence changes of a cpGFP to ligand-binding-induced conformational changes of the 5-HT2AR (Dong et al. 2021). PsychLight can categorize compounds into weakly or non-5-HT2AR binding, hallucinogens, and nonhallucinogens by real-time fluorescent readout (**Figure 4*d***). The novel compound AAZ-A-154 was discovered by the assay to be a nonhallucinogen. The nonhallucinogenic property of AAZ-A-154 was then validated in vivo with the head-twitch response (HTR) experiment in mice. With the forced swim and glucose preference tests in a genetic model of depression, AAZ-A-154 was shown to be a nonhallucinogenic psychedelic analog that exhibits antidepressant properties.

The genetically encoded approach to designing sensors also has the advantage of being able to study the action of a drug on receptors in vivo. Together with fiber photometry recording, psychLight signals are able to correlate 5-MeO-DMT action in medial prefrontal cortex (mPFC) during the HTR experiment. An intraperitoneal injection of 5-MeO-DMT takes about a minute to reach mPFC and initiate head twitching (**Figure 4*e***). With GPCR-based sensors directly monitoring drug actions in vivo, PBP-based sensors can have a major role in neuropharmacology as well, for example, by monitoring NM release induced by exogeneous drugs.

SUMMARY AND OUTLOOK

The development of genetically encoded sensors has opened doors in neuroscience research that were previously untenable, particularly in the context of understanding neural circuit bases of complex, naturalistic behavior. By reducing restrictions on animal model and experimental design, these sensors allow for the broadening of circuits- and systems-level neuroscience to encompass a larger array of questions and permit unprecedented exploration of neurobehavioral systems in real time.

To date, there are many NT/NMs lacking precise detection tools, including neuropeptides and lipid transmitters. By taking advantage of naturally designed GPCRs, a similar strategy to the GRAB and Light sensor–development pipeline can be generalized to cover more neurochemicals, which will greatly facilitate studies revealing their emergent roles under physiological and pathological conditions. In addition, the intrinsic properties of existing sensors demand further iterative optimization to be broadly applied with all microscopy techniques. The model we reported here provides theoretical guidance for future optimization. Sensor developers should utilize rational design and computational approaches, including machine learning, as applied in iSeroSnFR (Unger et al. 2020) or the recently developed AlphaFold 2.0 for protein structure prediction with unprecedented accuracy (Jumper et al. 2021, Tunyasuvunakool et al. 2021) to achieve these goals. Practically, a high-throughput screening system is crucial to maximize sensor optimization efficiency, since GPCR-based sensors can currently only be screened in mammalian cells. Fluorescence-activating cell sorting combined with image-based screening or the well-known CRISPR/Cas9 system that has been applied in the evolution of FPs and voltage sensors (Erdogan et al. 2020, Lee et al. 2020, Piatkevich et al. 2018) holds great promise for screening NT/NM sensors.

Extending the sensitivity, specificity, and color palette of NM sensors will continue to create rich opportunities for minimally invasive, multiplex imaging of neurochemical signaling dynamics. Together with advanced microscopy, opsin-based optogenetics, and cell atlas, fluorescent imaging with next-generation genetically encoded indicators will bring our experimental capabilities to a previously impossible level, thus uncovering brain mechanisms, and potentially transform our understanding of how neurochemical inputs influence cell and circuit function in health and disease.

DISCLOSURE STATEMENT

L.T. is a cofounder of Seven Biosciences. The other authors are not aware of any affiliations, memberships, funding, or financial holdings that might be perceived as affecting the objectivity of this review.

AUTHOR CONTRIBUTIONS

C.D. and L.T. generated the models and contributed to the Imaging Beyond Spikes with Neurotransmitter and Neuromodulator Sensors and Application of Neurotransmitter Sensors in Drug Discovery sections. Y.Z., Y.L., L.T., and C.D. contributed to Imaging Neuronal Activity

in Genetically Defined Populations, Imaging Beyond Spikes with Neurotransmitter and Neuromodulator Sensors, and Workflow for Development and Optimization of Neurotransmitter and Neuromodulator Sensors sections. K.L.-I., E.C.W., Y.Z., Y.L., and L.T. contributed to the Imaging Neuromodulator Release in Behaving Animals section.

ACKNOWLEDGMENTS

The authors would like to thank Dr. Alessio Andreoni for his critiques and helpful comments on modeling, and Dr. Weizhe Hong for providing **Figure 4*c***. This work was supported by the National Institutes of Health BRAIN Initiative (NS1133295, R21EY031858, and NS120824), Human Frontier Research Grant (L.T.), 2R01MH101214-06 (L.T.), T32MH112507 (K.L.-I.), and 1F32MMH125597-01A1 (E.C.W.), Beijing Municipal Science & Technology Commission (Z181100001318002 and Z181100001518004), and the National Science Fund for Distinguished Young Scholars of China.

LITERATURE CITED

Abdelfattah AS, Kawashima T, Singh A, Novak O, Liu H, et al. 2019. Bright and photostable chemigenetic indicators for extended in vivo voltage imaging. *Science* 365:699–704

Akerboom J, Carreras Calderon N, Tian L, Wabnig S, Prigge M, et al. 2013. Genetically encoded calcium indicators for multi-color neural activity imaging and combination with optogenetics. *Front. Mol. Neurosci.* 6:2

Andreoni A, Davis CMO, Tian L. 2019. Measuring brain chemistry using genetically encoded fluorescent sensors. *Curr. Opin. Biomed. Eng.* 12:59–67

Baird GS, Zacharias DA, Tsien RY. 1999. Circular permutation and receptor insertion within green fluorescent proteins. *PNAS* 96:11241–46

Borden PM, Zhang P, Shivange AV, Marvin JS, Cichon J, et al. 2020. A fast genetically encoded fluorescent sensor for faithful in vivo acetylcholine detection in mice, fish, worms and flies. bioRxiv 2020.02.07.939504. **https://doi.org/10.1101/2020.02.07.939504**

Bouabe H, Okkenhaug K. 2013. Gene targeting in mice: a review. *Methods Mol. Biol.* 1064:315–36

Broussard GJ, Liang Y, Fridman M, Unger EK, Meng G, et al. 2018. In vivo measurement of afferent activity with axon-specific calcium imaging. *Nat. Neurosci.* 21:1272–80

Cameron LP, Tombari RJ, Lu J, Pell AJ, Hurley ZQ, et al. 2021. A non-hallucinogenic psychedelic analogue with therapeutic potential. *Nature* 589:474–79

Chen T-W, Wardill TJ, Sun Y, Pulver SR, Renninger SL, et al. 2013. Ultrasensitive fluorescent proteins for imaging neuronal activity. *Nature* 499:295–300

Chen Y, Jang H, Spratt P, Kosar S, Taylor DE, et al. 2020. Soma-targeted imaging of neural circuits by ribosome tethering. *Neuron* 107(3):454–69.e6

Chi T, Gold JA. 2020. A review of emerging therapeutic potential of psychedelic drugs in the treatment of psychiatric illnesses. *J. Neurol. Sci.* 411:116715

Condon AF, Robinson BG, Asad N, Dore TM, Tian L, Williams JT. 2021. The residence of synaptically released dopamine on D2 autoreceptors. *Cell Rep.* 36:109465

Dalangin R, Drobizhev M, Molina RS, Aggarwal A, Patel R, et al. 2020. Far-red fluorescent genetically encoded calcium ion indicators. bioRxiv 2020.11.12.380089. **https://doi.org/10.1101/2020.11.12.380089**

Dana H, Mohar B, Sun Y, Narayan S, Gordus A, et al. 2016. Sensitive red protein calcium indicators for imaging neural activity. *eLife* 5:e12727

Dana H, Sun Y, Mohar B, Hulse BK, Kerlin AM, et al. 2019. High-performance calcium sensors for imaging activity in neuronal populations and microcompartments. *Nat. Methods* 16:649–57

Dong A, He K, Dudok B, Farrell JS, Guan W, et al. 2020. A fluorescent sensor for spatiotemporally resolved endocannabinoid dynamics in vitro and in vivo. bioRxiv 2020.10.08.329169. **https://doi.org/10.1101/2020.10.08.329169**

Dong C, Ly C, Dunlap LE, Vargas MV, Sun J, et al. 2021. Psychedelic-inspired drug discovery using an engineered biosensor. *Cell* 184:2779–92.e18

El-Husseini AE-D, Craven SE, Brock SC, Bredt DS. 2001. Polarized targeting of peripheral membrane proteins in neurons. *J. Biol. Chem.* 276:44984–92

Erdogan M, Fabritius A, Basquin J, Griesbeck O. 2020. Targeted in situ protein diversification and intra-organelle validation in mammalian cells. *Cell Chem. Biol.* 27:610–21.e5

Farrell JS, Colangeli R, Dong A, George AG, Addo-Osafo K, et al. 2021. In vivo endocannabinoid dynamics at the timescale of physiological and pathological neural activity. *Neuron* 109:2398–403.e4

Feng J, Zhang C, Lischinsky JE, Jing M, Zhou J, et al. 2019. A genetically encoded fluorescent sensor for rapid and specific in vivo detection of norepinephrine. *Neuron* 102:745–61.e8

Gong Y, Huang C, Li JZ, Grewe BF, Zhang Y, et al. 2015. High-speed recording of neural spikes in awake mice and flies with a fluorescent voltage sensor. *Science* 350:1361–66

Grienberger C, Konnerth A. 2012. Imaging calcium in neurons. *Neuron* 73:862–85

Guillaumin MCC, Burdakov D. 2021. Neuropeptides as primary mediators of brain circuit connectivity. *Front. Neurosci.* 15:644313

Gunaydin LA, Grosenick L, Finkelstein JC, Kauvar IV, Fenno LE, et al. 2014. Natural neural projection dynamics underlying social behavior. *Cell* 157:1535–51

Hauser AS, Attwood MM, Rask-Andersen M, Schioth HB, Gloriam DE. 2017. Trends in GPCR drug discovery: new agents, targets and indications. *Nat. Rev. Drug Discov.* 16:829–42

He Z, Zhang L, Hou W, Zhang X, Young LJ, et al. 2021. Paraventricular nucleus oxytocin subsystems promote active paternal behaviors in mandarin voles. *J. Neurosci.* 41:6699–713

Helassa N, Durst CD, Coates C, Kerruth S, Arif U, et al. 2018. Ultrafast glutamate sensors resolve high-frequency release at Schaffer collateral synapses. *PNAS* 115:5594–99

Hu H, Wei Y, Wang D, Su N, Chen X, et al. 2018. Glucose monitoring in living cells with single fluorescent protein-based sensors. *RSC Adv.* 8:2485–89

Hung LW, Neuner S, Polepalli JS, Beier KT, Wright M, et al. 2017. Gating of social reward by oxytocin in the ventral tegmental area. *Science* 357:1406–11

Inoue M, Takeuchi A, Manita S, Horigane SI, Sakamoto M, et al. 2019. Rational engineering of XCaMPs, a multicolor GECI suite for in vivo imaging of complex brain circuit dynamics. *Cell* 177:1346–60.e24

Jin L, Han Z, Platisa J, Wooltorton JRA, Cohen LB, Pieribone VA. 2012. Single action potentials and subthreshold electrical events imaged in neurons with a fluorescent protein voltage probe. *Neuron* 75:779–85

Jing M, Li Y, Zeng J, Huang P, Skirzewski M, et al. 2020. An optimized acetylcholine sensor for monitoring in vivo cholinergic activity. *Nat. Methods* 17:1139–46

Jing M, Zhang P, Wang G, Feng J, Mesik L, et al. 2018. A genetically encoded fluorescent acetylcholine indicator for in vitro and in vivo studies. *Nat. Biotechnol.* 36:726–37

Jumper J, Evans R, Pritzel A, Green T, Figurnov M, et al. 2021. Highly accurate protein structure prediction with AlphaFold. *Nature* 596:583–89

Keller JP, Marvin JS, Lacin H, Lemon WC, Shea J, et al. 2021. In vivo glucose imaging in multiple model organisms with an engineered single-wavelength sensor. *Cell Rep.* 35:109284

Kelly CR, Sharif NA. 2006. Pharmacological evidence for a functional serotonin-2B receptor in a human uterine smooth muscle cell line. *J. Pharmacol. Exp. Ther.* 317:1254–61

Kim H, Kim M, Im S-K, Fang S. 2018. Mouse Cre-LoxP system: general principles to determine tissue-specific roles of target genes. *Lab Anim. Res.* 34:147–59

Kingsbury L, Huang S, Wang J, Gu K, Golshani P, et al. 2019. Correlated neural activity and encoding of behavior across brains of socially interacting animals. *Cell* 178:429–46.e16

Knopfel T, Song C. 2019. Optical voltage imaging in neurons: moving from technology development to practical tool. *Nat. Rev. Neurosci.* 20:719–27

Kovacs GL. 2004. The endocrine brain: pathophysiological role of neuropeptide-neurotransmitter interactions. *EJIFCC* 15:107–12

Kralj JM, Douglass AD, Hochbaum DR, Maclaurin D, Cohen AE. 2011. Optical recording of action potentials in mammalian neurons using a microbial rhodopsin. *Nat. Methods* 9:90–95

Kügler S, Kilic E, Bähr M. 2003. Human synapsin 1 gene promoter confers highly neuron-specific long-term transgene expression from an adenoviral vector in the adult rat brain depending on the transduced area. *Gene. Ther.* 10:337–47

Lee J, Liu Z, Suzuki PH, Ahrens JF, Lai S, et al. 2020. Versatile phenotype-activated cell sorting. *Sci. Adv.* 6:eabb7438

Lee SJ, Lodder B, Chen Y, Patriarchi T, Tian L, Sabatini BL. 2021. Cell-type-specific asynchronous modulation of PKA by dopamine in learning. *Nature* 590:451–56

Lim MM, Young LJ. 2006. Neuropeptidergic regulation of affiliative behavior and social bonding in animals. *Horm. Behav.* 50:506–17

Lobas MA, Tao R, Nagai J, Kronschlager MT, Borden PM, et al. 2019. A genetically encoded single-wavelength sensor for imaging cytosolic and cell surface ATP. *Nat. Commun.* 10:711

Mank M, Santos AF, Direnberger S, Mrsic-Flogel TD, Hofer SB, et al. 2008. A genetically encoded calcium indicator for chronic in vivo two-photon imaging. *Nat. Methods* 5:805–11

Marvin JS, Borghuis BG, Tian L, Cichon J, Harnett MT, et al. 2013. An optimized fluorescent probe for visualizing glutamate neurotransmission. *Nat. Methods* 10:162–70

Marvin JS, Scholl B, Wilson DE, Podgorski K, Kazemipour A, et al. 2018. Stability, affinity, and chromatic variants of the glutamate sensor iGluSnFR. *Nat. Methods* 15:936–39

Marvin JS, Shimoda Y, Magloire V, Leite M, Kawashima T, et al. 2019. A genetically encoded fluorescent sensor for in vivo imaging of GABA. *Nat. Methods* 16:763–70

Matthews T, Danese A, Wertz J, Odgers CL, Ambler A, et al. 2016. Social isolation, loneliness and depression in young adulthood: a behavioural genetic analysis. *Soc. Psychiatry Psychiatr. Epidemiol.* 51:339–48

Mita M, Ito M, Harada K, Sugawara I, Ueda H, et al. 2019. Green fluorescent protein-based glucose indicators report glucose dynamics in living cells. *Anal. Chem.* 91:4821–30

Miyawaki A, Llopis J, Heim R, McCaffery JM, Adams JA, et al. 1997. Fluorescent indicators for Ca^{2+} based on green fluorescent proteins and calmodulin. *Nature* 388:882–87

Mohebi A, Pettibone JR, Hamid AA, Wong J-MT, Vinson LT, et al. 2019. Dissociable dopamine dynamics for learning and motivation. *Nature* 570:65–70

Motulsky HJ, Neubig RR. 2010. Analyzing binding data. *Curr. Protocols Neurosci.* 52:7.5.1–65

Mueller KL, Hoon MA, Erlenbach I, Chandrashekar J, Zuker CS, Ryba NJP. 2005. The receptors and coding logic for bitter taste. *Nature* 434:225–29

Muir J, Lorsch ZS, Ramakrishnan C, Deisseroth K, Nestler EJ, et al. 2018. In vivo fiber photometry reveals signature of future stress susceptibility in nucleus accumbens. *Neuropsychopharmacology* 43:255–63

Nadim F, Bucher D. 2014. Neuromodulation of neurons and synapses. *Curr. Opin. Neurobiol.* 29:48–56

Nagai T, Sawano A, Park ES, Miyawaki A. 2001. Circularly permuted green fluorescent proteins engineered to sense Ca^{2+}. *PNAS* 98:3197–202

Nagai T, Yamada S, Tominaga T, Ichikawa M, Miyawaki A. 2004. Expanded dynamic range of fluorescent indicators for Ca^{2+} by circularly permuted yellow fluorescent proteins. *PNAS* 101:10554–59

Nakai J, Ohkura M, Imoto K. 2001. A high signal-to-noise Ca^{2+} probe composed of a single green fluorescent protein. *Nat. Biotechnol.* 19:137–41

Nieuwenhuis B, Haenzi B, Hilton S, Carnicer-Lombarte A, Hobo B, et al. 2021. Optimization of adeno-associated viral vector-mediated transduction of the corticospinal tract: comparison of four promoters. *Gene Ther.* 28:56–74

Olsen RHJ, DiBerto JF, English JG, Glaudin AM, Krumm BE, et al. 2020. TRUPATH, an open-source biosensor platform for interrogating the GPCR transducerome. *Nat. Chem. Biol.* 16:841–49

Pal A, Tian L. 2020. Imaging voltage and brain chemistry with genetically encoded sensors and modulators. *Curr. Opin. Chem. Biol.* 57:166–76

Palmer AE, Giacomello M, Kortemme T, Hires SA, Lev-Ram V, et al. 2006. Ca^{2+} indicators based on computationally redesigned calmodulin-peptide pairs. *Chem. Biol.* 13:521–30

Panzera LC, Hoppa MB. 2019. Genetically encoded voltage indicators are illuminating subcellular physiology of the axon. *Front Cell Neurosci* 13:52

Patriarchi T, Cho JR, Merten K, Howe MW, Marley A, et al. 2018. Ultrafast neuronal imaging of dopamine dynamics with designed genetically encoded sensors. *Science* 360:aat4422

Patriarchi T, Mohebi A, Sun J, Marley A, Liang R, et al. 2020. An expanded palette of dopamine sensors for multiplex imaging in vivo. *Nat. Methods* 17:1147–55

Peng W, Wu Z, Song K, Zhang S, Li Y, Xu M. 2020. Regulation of sleep homeostasis mediator adenosine by basal forebrain glutamatergic neurons. *Science* 369:eabb0556

Piatkevich KD, Jung EE, Straub C, Linghu C, Park D, et al. 2018. A robotic multidimensional directed evolution approach applied to fluorescent voltage reporters. *Nat. Chem. Biol.* 14:352–60

Qian Y, Orozco Cosio DM, Piatkevich KD, Aufmkolk S, Su WC, et al. 2020. Improved genetically encoded near-infrared fluorescent calcium ion indicators for in vivo imaging. *PLOS Biol.* 18:e3000965

Qian Y, Piatkevich KD, McLarney B, Abdelfattah AS, Mehta S, et al. 2019. A genetically encoded near-infrared fluorescent calcium ion indicator. *Nat. Methods* 16:171–74

Quiocho FA, Ledvina PS. 1996. Atomic structure and specificity of bacterial periplasmic receptors for active transport and chemotaxis: variation of common themes. *Mol. Microbiol.* 20:17–25

Rasmussen M, Kong L, Zhang G-R, Liu M, Wang X, et al. 2007. Glutamatergic or GABAergic neuron-specific, long-term expression in neocortical neurons from helper virus-free HSV-1 vectors containing the phosphate-activated glutaminase, vesicular glutamate transporter-1, or glutamic acid decarboxylase promoter. *Brain Res.* 1144:19–32

Sabatini BL, Tian L. 2020. Imaging neurotransmitter and neuromodulator dynamics in vivo with genetically encoded indicators. *Neuron* 108:17–32

Sadakane O, Masamizu Y, Watakabe A, Terada S-I, Ohtsuka M, et al. 2015. Long-term two-photon calcium imaging of neuronal populations with subcellular resolution in adult non-human primates. *Cell Rep.* 13:1989–99

Seidemann E, Chen Y, Bai Y, Chen SC, Mehta P, et al. 2016. Calcium imaging with genetically encoded indicators in behaving primates. *eLife* 5:e16178

Shcherbakova DM, Shemetov AA, Kaberniuk AA, Verkhusha VV. 2015. Natural photoreceptors as a source of fluorescent proteins, biosensors, and optogenetic tools. *Annu. Rev. Biochem.* 84:519–50

Shemetov AA, Monakhov MV, Zhang Q, Canton-Josh JE, Kumar M, et al. 2021. A near-infrared genetically encoded calcium indicator for in vivo imaging. *Nat. Biotechnol.* 39:368–77

Shen Y, Dana H, Abdelfattah AS, Patel R, Shea J, et al. 2018. A genetically encoded Ca^{2+} indicator based on circularly permutated sea anemone red fluorescent protein eqFP578. *BMC Biol.* 16:9

Shivange AV, Borden PM, Muthusamy AK, Nichols AL, Bera K, et al. 2019. Determining the pharmacokinetics of nicotinic drugs in the endoplasmic reticulum using biosensors. *J. Gen. Physiol.* 151:738–57

Shoichet BK, Kobilka BK. 2012. Structure-based drug screening for G-protein-coupled receptors. *Trends Pharmacol. Sci.* 33:268–72

Smith JS, Lefkowitz RJ, Rajagopal S. 2018. Biased signalling: from simple switches to allosteric microprocessors. *Nat. Rev. Drug Discov.* 17:243–60

St-Pierre F, Marshall JD, Yang Y, Gong Y, Schnitzer MJ, Lin MZ. 2014. High-fidelity optical reporting of neuronal electrical activity with an ultrafast fluorescent voltage sensor. *Nat. Neurosci.* 17:884–89

Sun F, Zeng J, Jing M, Zhou J, Feng J, et al. 2018. A genetically encoded fluorescent sensor enables rapid and specific detection of dopamine in flies, fish, and mice. *Cell* 174:481–96.e19

Sun F, Zhou J, Dai B, Qian T, Zeng J, et al. 2020. Next-generation GRAB sensors for monitoring dopaminergic activity in vivo. *Nat. Methods* 17:1156–66

Sung YM, Wilkins AD, Rodriguez GJ, Wensel TG, Lichtarge O. 2016. Intramolecular allosteric communication in dopamine D2 receptor revealed by evolutionary amino acid covariation. *PNAS* 113(13):3539–44

Tai F, Wang TZ. 2001. Social organization of mandarin voles in burrow system. *Acta Theriol. Sin.* 21:50–56

Tai F, Wang TZ, Zhao YJ. 2001. Mating system of mandarin vole (*Microtus mandarinus*). *Acta Zool. Sin.* 47:260–67

Tanaka M, Sun F, Li Y, Mooney R. 2018. A mesocortical dopamine circuit enables the cultural transmission of vocal behaviour. *Nature* 563:117–20

Tian L, Hires SA, Mao T, Huber D, Chiappe ME, et al. 2009. Imaging neural activity in worms, flies and mice with improved GCaMP calcium indicators. *Nat. Methods* 6:875–81

Tikhonova IG, Costanzi S. 2009. Unraveling the structure and function of G protein-coupled receptors through NMR spectroscopy. *Curr. Pharm. Des.* 15:4003–16

Trainor BC, Pride MC, Landeros RV, Knoblauch NW, Takahashi EY, et al. 2011. Sex differences in social interaction behavior following social defeat stress in the monogamous California mouse (*Peromyscus californicus*). *PLOS ONE* 6:e17405

Tunyasuvunakool K, Adler J, Wu Z, Green T, Zielinski M, et al. 2021. Highly accurate protein structure prediction for the human proteome. *Nature* 596:590–96

Unger EK, Keller JP, Altermatt M, Liang R, Matsui A, et al. 2020. Directed evolution of a selective and sensitive serotonin sensor via machine learning. *Cell* 183:1986–2002.e26

Villette V, Chavarha M, Dimov IK, Bradley J, Pradhan L, et al. 2019. Ultrafast two-photon imaging of a high-gain voltage indicator in awake behaving mice. *Cell* 179:1590–608.e23

Wan J, Peng W, Li X, Qian T, Song K, et al. 2021. A genetically encoded sensor for measuring serotonin dynamics. *Nat. Neurosci.* 24:746–52

Wang H, Jing M, Li Y. 2018. Lighting up the brain: genetically encoded fluorescent sensors for imaging neurotransmitters and neuromodulators. *Curr. Opin. Neurobiol.* 50:171–78

Wang W, Kim CK, Ting AY. 2019. Molecular tools for imaging and recording neuronal activity. *Nat. Chem. Biol.* 15:101–10

Wang X, Zhang C, Szábo G, Sun Q-Q. 2013. Distribution of CaMKIIα expression in the brain in vivo, studied by CaMKIIα-GFP mice. *Brain Res.* 1518:9–25

Whalen EJ, Rajagopal S, Lefkowitz RJ. 2011. Therapeutic potential of β-arrestin- and G protein-biased agonists. *Trends Mol. Med.* 17:126–39

Wright EC, Hostinar CE, Trainor BC. 2020. Anxious to see you: neuroendocrine mechanisms of social vigilance and anxiety during adolescence. *Eur. J. Neurosci.* 52:2516–29

Wu J, Abdelfattah AS, Zhou H, Ruangkittisakul A, Qian Y, et al. 2018. Genetically encoded glutamate indicators with altered color and topology. *ACS Chem. Biol.* 13:1832–37

Wu Z, He K, Chen Y, Li H, Pan S, et al. 2021. An ultrasensitive GRAB sensor for detecting extracellular ATP in vitro and vivo. bioRxiv 2021.02.24.432680. **https://doi.org/10.1101/2021.02.24.432680**

Yang HH, St-Pierre F, Sun X, Ding X, Lin MZ, Clandinin TR. 2016. Subcellular imaging of voltage and calcium signals reveals neural processing in vivo. *Cell* 166:245–57

Zhang D, Zhao Q, Wu B. 2015. Structural studies of G protein-coupled receptors. *Mol. Cells* 38:836–42

Zhang L, Liang B, Barbera G, Hawes S, Zhang Y, et al. 2019. Miniscope GRIN lens system for calcium imaging of neuronal activity from deep brain structures in behaving animals. *Curr. Protoc. Neurosci.* 86:e56

Zhang Y, Rózsa M, Bushey D, Zheng J, Reep D, et al. 2020. *jGCaMP8 fast genetically encoded calcium indicators*. Inf. Sheet, Janelia, Boston, MA

Zhao Y, Araki S, Wu J, Teramoto T, Chang YF, et al. 2011. An expanded palette of genetically encoded Ca^{2+} indicators. *Science* 333:1888–91

Ziv Y, Ghosh KK. 2015. Miniature microscopes for large-scale imaging of neuronal activity in freely behaving rodents. *Curr. Opin. Neurobiol.* 32:141–47